nature nanotechnology

LETTERS

PUBLISHED ONLINE: 3 APRIL 2017 | DOI: 10.1038/NNANO.2017.21

Tunable sieving of ions using graphene oxide membranes

Jijo Abraham[1,2,3†], Kalangi S. Vasu[1,2†], Christopher D. Williams[2], Kalon Gopinadhan[3], Yang Su[1,2], Christie T. Cherian[1,2], James Dix[2], Eric Prestat[4], Sarah J. Haigh[4], Irina V. Grigorieva[1], Paola Carbone[2], Andre K. Geim[3] and Rahul R. Nair[1,2*]

Graphene oxide membranes show exceptional molecular permeation properties, with promise for many applications[1–5]. However, their use in ion sieving and desalination technologies is limited by a permeation cutoff of ~9 Å (ref. 4), which is larger than the diameters of hydrated ions of common salts[4,6]. The cutoff is determined by the interlayer spacing (*d*) of ~13.5 Å, typical for graphene oxide laminates that swell in water[2,4]. Achieving smaller *d* for the laminates immersed in water has proved to be a challenge. Here, we describe how to control *d* by physical confinement and achieve accurate and tunable ion sieving. Membranes with *d* from ~9.8 Å to 6.4 Å are demonstrated, providing a sieve size smaller than the diameters of hydrated ions. In this regime, ion permeation is found to be thermally activated with energy barriers of ~10–100 kJ mol^{-1} depending on *d*. Importantly, permeation rates decrease exponentially with decreasing sieve size but water transport is weakly affected (by a factor of <2). The latter is attributed to a low barrier for the entry of water molecules and large slip lengths inside graphene capillaries. Building on these findings, we demonstrate a simple scalable method to obtain graphene-based membranes with limited swelling, which exhibit 97% rejection for NaCl.

Selectively permeable membranes with subnanometre pores attract strong interest due to their analogous behaviour with biological membranes and potential applications in water filtration, molecular separation and desalination[7–14]. Nanopores with sizes comparable to, or smaller than, the diameter *D* of hydrated ions are predicted to show enhanced ion selectivity[14–18] because of dehydration required for the permeation of ions through such atomic-scale sieves. Despite extensive research on ion dehydration effects[9,14–19], experimental investigation of the ion sieving controlled by dehydration has been limited because of difficulties in fabricating uniform membranes with well-defined subnanometre pores. The realization of membranes with dehydration-assisted selectivity would be a significant step forward. So far, research into novel membranes has mostly focused on improving the water flux rather than on ion selectivity. On the other hand, modelling of practically relevant filtration processes shows that an increase in water permeation rates above the rates currently achieved (2–3 l m^{-2} h^{-1} bar^{-1}) would not contribute greatly to the overall efficiency of desalination[13,20,21]. Alternative approaches based on higher water-ion selectivity may open new possibilities for improving filtration technologies, as the performance of state-of-the-art membranes is currently limited by the solution-diffusion mechanism, in which water molecules dissolve in the membrane material and then diffuse across the membrane[13]. Recently, carbon nanomaterials including carbon nanotubes and graphene have emerged as promising membrane materials. Unfortunately, such membranes are difficult to manufacture on an industrial scale[10,11,13,22]. In particular, monolayer graphene was suggested as a membrane for ion exclusion by creating subnanometre pores using ion bombardment and selective etching[7–10]. However, it is difficult to achieve the high density and uniformity of such pores, which is required for industrial applications, because of the stochastic nature of the involved processes. In contrast, graphene oxide (GO), a chemical derivative of graphene with oxygen functionalities[23], has attracted widespread interest due to its exceptional water permeation and molecular sieving properties[1,2,4] as well as realistic prospects for industrial-scale production[3,5]. Molecular permeation through GO membranes is believed to occur along a network of pristine graphene channels that develop between functionalized areas of GO sheets[1] (typically, an area of 40–60% remains free from functionalization[24,25]), and their sieving properties are defined by the interlayer spacing, *d*, which depends on the humidity of the surroundings[1,4]. Immersing GO membranes in liquid water leads to intercalation of 2–3 layers of water molecules between individual GO sheets, which results in swelling and $d \approx 13.5$ Å. A number of strategies have been tried to inhibit the swelling effect, including partial reduction of GO (ref. 26), ultraviolet reduction of GO–titania hybrid membranes[27] and covalent crosslinking[28–30]. In this Letter, we investigate ion permeation through GO laminates with *d* controlled from ≈9.8 to ≈6.4 Å, which is achieved by physical confinement (Fig. 1a).

Thick (≈100 μm) GO laminates prepared as reported previously[1] were cut into rectangular strips (4 mm × 10 mm) and stored for 1 to 2 weeks at different relative humidities (RH), achieved using saturated salt solutions[1,31]. The resulting interlayer spacing (Fig. 1e) was varied from ≈6.4 to 9.8 Å with RH changing from 0 to 100%. GO laminates soaked in liquid water showed $d \approx 13.7 \pm 0.3$ Å. All these values agree with previous reports, where the changes in *d* were attributed to successive incorporation of water molecules into various sites between GO sheets[32]. Individual GO strips with desirable *d* were then encapsulated and stacked together using Stycast epoxy as shown in Fig. 1b,c to increase the available cross-section for filtration to ~1 mm (see Methods and Supplementary Fig. 1). The stacked GO laminates, embedded in the epoxy (Fig. 1c), are referred to as physically confined GO (PCGO) membranes because the epoxy mechanically restricts the swelling of the laminate on exposure to RH or liquid water (see Methods). The stacks were glued into a slot made in either a metal or plastic plate (Fig. 1b). Two sides of these stacked PCGO membranes were then trimmed off to make sure that all the nanochannels

[1]National Graphene Institute, University of Manchester, Manchester M13 9PL, UK. [2]School of Chemical Engineering and Analytical Science, University of Manchester, Manchester M13 9PL, UK. [3]School of Physics and Astronomy, University of Manchester, Manchester M13 9PL, UK. [4]School of Materials, University of Manchester, Manchester M13 9PL, UK. †These authors contributed equally to this work. *e-mail: rahul@manchester.ac.uk

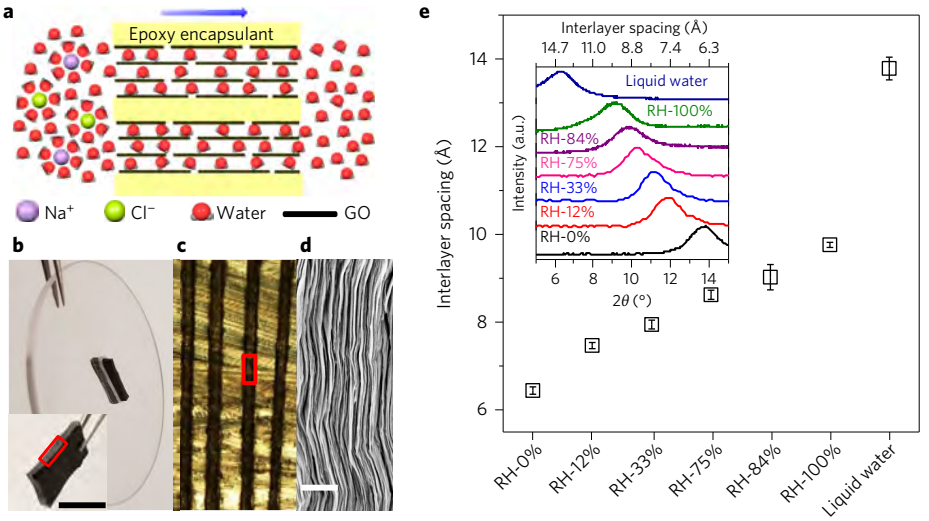

Figure 1 | Physically confined GO membranes with tunable interlayer spacing. a, Schematic illustrating the direction of ion/water permeation along graphene planes. **b**, Photograph of a PCGO membrane glued into a rectangular slot within a plastic disk of 5 cm in diameter. Inset: photo of the PCGO stack before it was placed inside the slot. Scale bar, 5 mm. **c**, Optical micrograph of the cross-sectional area marked by a red rectangle in **b**, which shows 100-μm-thick GO laminates (black) embedded in epoxy. Epoxy is seen in light yellow with dark streaks because of surface scratches. **d**, Scanning electron microscopy image from the marked region in **c**. Scale bar, 1 μm. **e**, Humidity-dependent interlayer spacing, *d*, found using X-ray diffraction (inset). The case of liquid water is also shown. Error bars denote standard deviations using at least two measurements from three different samples.

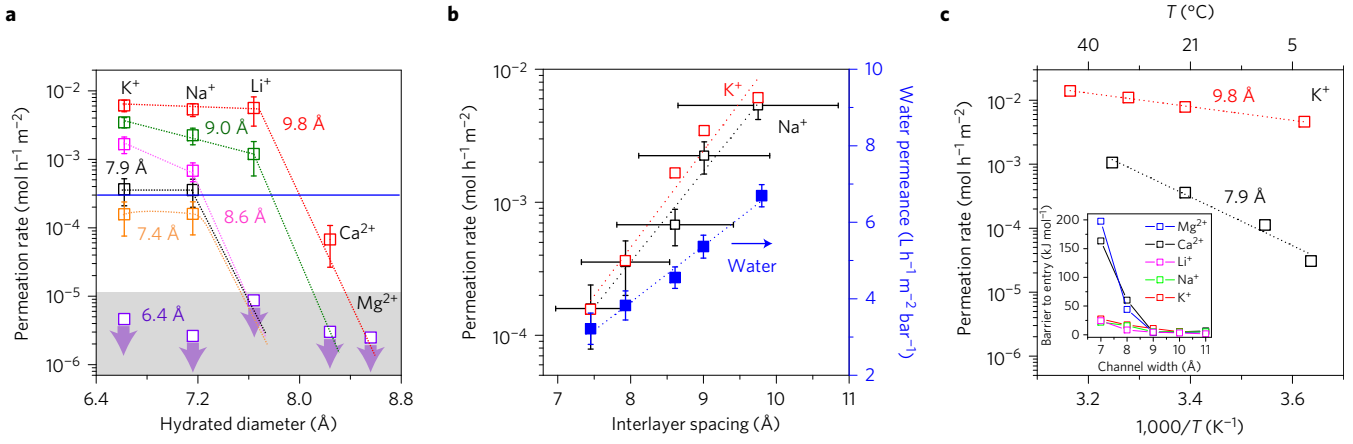

Figure 2 | Tunable ion sieving. a, Permeation rates through PCGO membranes with different interlayer distances (colour coded). The salts used were KCl, NaCl, LiCl, $CaCl_2$ and $MgCl_2$. The hydrated diameters are taken from ref. 6 (Supplementary Section 4). Dashed lines are guides to the eye indicating a rapid cutoff in salt permeation, which is dependent on the interlayer spacing, *d*. Grey area shows the below-detection limit for our measurements lasting five days, with arrows indicating the limits for individual salts. The horizontal blue line indicates our detection limit for Cl^-. Above the latter limit, we found that both cations and anions permeated in stoichiometric quantities. Error bars denote standard deviation. **b**, Permeation rates for K^+ and Na^+ depend exponentially on the interlayer distance (left axis). Water permeation varied only linearly with *d* (blue squares, right axis). The dotted lines are best fits. The horizontal error bars correspond to a half-width for the diffractions peaks in Fig. 1e and are same for all the three data sets. The vertical error bars indicate the standard deviation. The errors for K^+ are similar to those for Na^+ and have been omitted for clarity. **c**, Temperature dependence for K^+ permeation. Dotted lines are best fits to the Arrhenius behaviour. Inset: energy barriers for various ions and different *d*, as found in our molecular dynamics simulations.

were open (Fig. 1d) before carrying out permeation experiments, in which ions and water molecules permeate along the lamination direction as shown in Fig. 1a.

Our measurement set-up was similar to the one previously reported[4] and consisted of two Teflon compartments (feed and permeate) separated by a PCGO membrane (Supplementary Fig. 2). The feed and permeate compartments were filled with 10 ml of a salt solution and deionized water, respectively. As expected, the ion concentration in the permeate compartment increases with time and with increasing concentration of the feed solution (Supplementary Section 3 and Supplementary Fig. 3). Figure 2a summarizes our results obtained for various ions permeating through PCGO membranes with different interlayer spacing. One can see that the permeation rates and the cutoff diameter for salt permeation decrease monotonically with decreasing *d*. Membranes with $d \approx 6.4$ Å showed no detectable ion concentration in the permeate even after 5 days. This further confirms that our PCGO membranes do not swell in water over time, despite a finite mechanical rigidity of the epoxy confinement. When plotted as a function of *d*, the observed ion permeation rates for Na^+ and K^+ showed an exponential dependence, decreasing by two orders of magnitude as *d* decreased from 9.8 to 7.4 Å (Fig. 2b). In contrast, the same PCGO membranes (Supplementary Section 5) showed only a little variation in permeation rates for water (Fig. 2b),

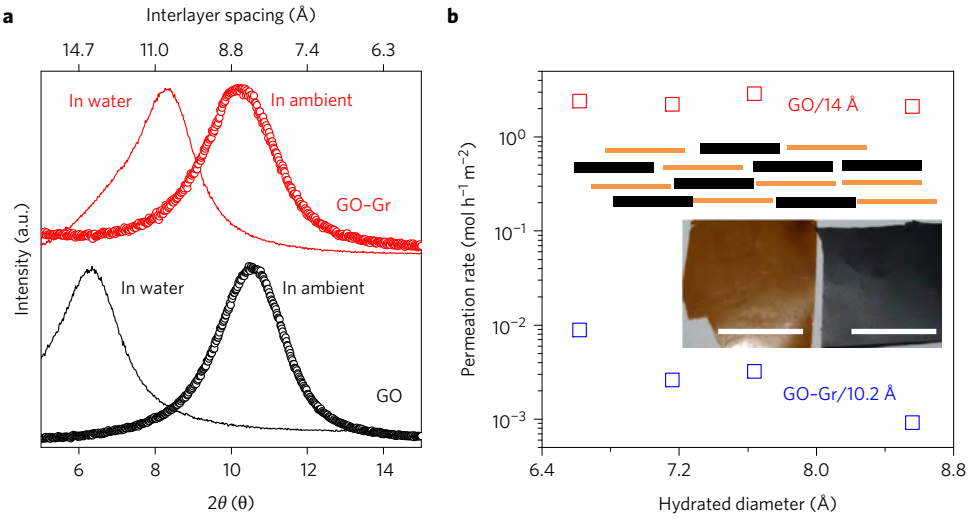

Figure 3 | Graphene oxide membrane with limited swelling. a, X-ray diffraction showing shifts of the (001) peak due to swelling in liquid water for the standard GO laminate and a composite made from graphene and graphene oxide (GO–Gr). **b**, Ion permeation rates (same salts as in Fig. 2) through such GO ($d \approx 14$ Å) and GO–Gr ($d \approx 10.2$ Å) membranes with a thickness of 5 μm. Top inset: schematic of the GO–Gr structure (brown blocks, GO; black, graphene). Bottom inset: photographs of GO and GO–Gr membranes (left, and right, respectively). Scale bars, 1 cm.

decreasing by a factor of ≈2 for the same range of d. We note that this observation rules out that the exponential changes in ion permeation could be related to partial clogging of graphene capillaries.

Both the observed relatively high permeation rates for Li^+, K^+ and Na^+ for $d > 9$ Å and their exponential decay for smaller d are surprising. Indeed, when considering steric (size-exclusion) effects, it is often assumed that ions in water occupy a rigid volume given by their hydrated diameters D. If this simplification was accurate, our PCGO membranes should not allow permeation of any common salt. Indeed, the effective pore size δ can be estimated as $d - a$, where $a \approx 3.4$ Å is the thickness of graphene[1,33]. This yields $\delta \approx 6.4$ Å for our largest capillaries ($d \approx 9.8$ Å), which is smaller than D for all the ions in Fig. 2a. This clearly indicates that ion sieving is not purely a geometric effect. On the other hand, if we assume that hydrated ions do fit into the nanochannels and their permeation is only limited by diffusion through water, the expected permeation rates should be significantly higher than those observed experimentally. For classical diffusion the permeation rate J is given by

$$J = \text{Diff} \times \Delta C \times A_{\text{eff}}/L \quad (1)$$

where ΔC is the concentration gradient across the membrane (1 M for the experiments in Fig. 2), A_{eff} is the total cross-sectional area of nanocapillaries (≈3–8 mm^2), L is the diffusion length through the PCGO membrane (≈3 mm) and Diff is the diffusion coefficient for ions in water (typically, Diff ~10^{-5} cm^2 s^{-1}; see Supplementary Section 6). Equation (1) yields rates that are 2–4 orders magnitude higher than those shown in Fig. 2. This is in stark contrast to the sieving properties of GO laminates with $d \approx 13.5$ Å that showed an enhancement rather than suppression of ion diffusion[4]. Clearly, the fact that the available space δ in PCGO laminates becomes smaller than D pushes the permeating hydrated ions into a new regime, distinct both from ions moving through wider nanocapillaries and from permeation behaviour of pure water. In the latter case, as shown in Fig. 2b, permeation rates for water molecules (whose size is smaller than δ) are three orders of magnitude higher than those estimated from the standard Hagen–Poiseuille equation using non-slip boundary conditions and the given dimensions of nanocapillaries (Supplementary Section 5). Similar flow enhancement (by three orders of magnitude) was recently reported for artificial graphene capillaries and attributed to a large slip length of ~60 nm for water on graphene[33].

To gain an insight into the mechanism of ion permeation through our membranes, we carried out permeation experiments at different temperatures, T (Fig. 2c). For both channel sizes, $d = 9.8$ Å and $d = 7.9$ Å, the permeation rates follow the Arrhenius equation, $\exp(-E/k_BT)$, that is, show activation behaviour. Here, E is the energy barrier and k_B is the Boltzmann constant. The data yield $E = 72 \pm 7$ kJ mol^{-1} and 20 ± 2 kJ mol^{-1} for K^+ ion permeation through PCGO membranes with $d \approx 7.9$ and 9.8 Å, respectively. The exponential dependence explains the fact that the observed ion diffusion rates are orders of magnitude smaller than those given by equation (1), as at room temperature $E \gg k_BT$ for both channel sizes. The activation behaviour is also in agreement with recent theoretical predictions that nanopores with diameters <10 Å should exhibit significant energy barriers because of the required partial dehydration for the entry of ions[9,14–18]. Qualitatively, this mechanism can be explained as follows. In a bulk solution, water molecules stabilize ions by forming concentric hydration shells. For an ion to enter a channel with $\delta < D$, some water molecules must be removed from the hydration shell. The higher the ion charge, the stronger it attracts water molecules. Accordingly, ions with larger hydration free energies[34] and, therefore, 'tougher' water shells are expected to experience larger barriers for entry into atomic-scale capillaries and exponentially smaller permeation rates. Ions with weakly bound shells are easier to strip from their water molecules to allow their entry into nanochannels. Similar arguments can be used to understand why water does not exhibit any exponential dependence on d: water–water interactions are weak, so it costs relatively little energy to remove surrounding water from water molecules entering the capillaries[16].

To support the proposed mechanism of dehydration-limited ion permeation for our PCGO membranes, we employed the previously suggested model of a network of graphene capillaries, which was developed to account for the fast permeation of water through GO membranes[1,4,18]. Within this model, we performed molecular dynamics simulations to find energy barriers for various ions entering graphene capillaries of different widths (Supplementary Section 6). As seen in Fig. 2c the energy barrier E exhibits a sharp increase for $d < 9$ Å and is considerably larger for divalent ions compared with

monovalent ions, in agreement with our experiments and the above discussion (Fig. 2a). Quantitatively, the obtained E are of the same order of magnitude as those found experimentally; the discrepancy in exact values can be expected because realistic GO channels contain non-stoichiometric functionalities, rough edges and so on, which are difficult to model accurately. We also performed simulations to evaluate a possible contribution of diffusion rates through capillaries themselves to the overall permeation rates. Our results show that the diffusion coefficient for K^+ changes with d but the effect is small compared with the exponential decrease in permeation rates, which was observed experimentally (Supplementary Section 6). This suggests that the energy barrier associated with dehydration is the dominant effect in our case of subnanometre capillaries.

Finally, the exponential suppression of ion permeation combined with fast water transport in PCGO membranes make them an interesting candidate for water filtration applications. Even though scalable production of such membranes is difficult, one can envisage using alternative fabrication techniques to control d in GO laminates. To this end, we show that it is possible to restrict the swelling of GO membranes in liquid water, for example, simply by incorporating graphene (Gr) flakes into GO laminates (Supplementary Section 7). The resulting composites referred to as GO–Gr membranes exhibit notably less swelling (difference in d of ≈4 Å) with respect to the standard GO laminates (Fig. 3a). The observed large difference in d can be due to graphene's hydrophobicity that limits the water intake. The ion permeation rate through GO–Gr membranes was found to be suppressed by more than two orders of magnitude compared with GO (Fig. 3b), in agreement with the projected rates for the given extent of swelling if the exponential dependence of Fig. 2 is extrapolated. At the same time, water permeation rates are essentially unaffected by the incorporation of graphene into GO laminates (decrease only by 20%; Supplementary Section 7). The salt rejection properties of our GO–Gr membranes were further investigated using forward osmosis, where we employed concentrated sugar (3 M) and NaCl (0.1 M) solutions as the draw and feed solutions, respectively (Supplementary Section 7). Salt rejection was calculated as $1 - C_d/C_f$, where C_d and C_f are the concentration of NaCl at the draw and feed sides, respectively. Our analysis yielded ≈97% salt rejection for the GO–Gr membranes with a water flux of ≈0.5 l m^{-2} h^{-1}. Even though the flux is lower than 5–10 l m^{-2} h^{-1} typical for forward osmosis[35], we believe this characteristic can be significantly improved by decreasing the membrane thickness to 1 μm or less (Supplementary Section 7). Such thicknesses are readily achievable for GO laminates[2] and can result in fluxes >5 l m^{-2} h^{-1}.

In conclusion, we have demonstrated the possibility to control the interlayer spacing in GO membranes in the range below 10 Å. In this regime, the capillary size is smaller than the hydrated diameters of ions and their permeation is exponentially suppressed with decreasing d. The suppression mechanism can be described in terms of additional energy barriers that arise because of the necessity to partially strip ions from their hydrated shells so that they can fit inside the capillaries. Water transport is much less affected by d. Our work shows a possible route to the production of GO membranes with controllable interlayer spacing for desalination applications.

Methods

Methods and any associated references are available in the online version of the paper.

Received 29 September 2016; accepted 2 February 2017; published online 3 April 2017

References

1. Nair, R. R., Wu, H. A., Jayaram, P. N., Grigorieva, I. V. & Geim, A. K. Unimpeded permeation of water through helium-leak-tight graphene-based membranes. *Science* **335,** 442–444 (2012).
2. Sun, P. Z., Wang, K. L. & Zhu, H. W. Recent developments in graphene-based membranes: structure, mass-transport mechanism and potential applications. *Adv. Mater.* **28,** 2287–2310 (2016).
3. Liu, G. P., Jin, W. Q. & Xu, N. P. Graphene-based membranes. *Chem. Soc. Rev.* **44,** 5016–5030 (2015).
4. Joshi, R. K. *et al.* Precise and ultrafast molecular sieving through graphene oxide membranes. *Science* **343,** 752–754 (2014).
5. Akbari, A. *et al.* Large-area graphene-based nanofiltration membranes by shear alignment of discotic nematic liquid crystals of graphene oxide. *Nat. Commun.* **7,** 10891 (2016).
6. Tansel, B. Significance of thermodynamic and physical characteristics on permeation of ions during membrane separation: hydrated radius, hydration free energy and viscous effects. *Sep. Purif. Technol.* **86,** 119–126 (2012).
7. O'Hern, S. C. *et al.* Selective ionic transport through tunable subnanometer pores in single-layer graphene membranes. *Nano Lett.* **14,** 1234–1241 (2014).
8. Rollings, R. C., Kuan, A. T. & Golovchenko, J. A. Ion selectivity of graphene nanopores. *Nat. Commun.* **7,** 11408 (2016).
9. Jain, T. *et al.* Heterogeneous sub-continuum ionic transport in statistically isolated graphene nanopores. *Nat. Nanotech.* **10,** 1053–1057 (2015).
10. Surwade, S. P. *et al.* Water desalination using nanoporous single-layer graphene. *Nat. Nanotech.* **10,** 459–464 (2015).
11. Cohen-Tanugi, D. & Grossman, J. C. Water desalination across nanoporous graphene. *Nano Lett.* **12,** 3602–3608 (2012).
12. Wang, L. D. *et al.* Molecular valves for controlling gas phase transport made from discrete ångström-sized pores in graphene. *Nat. Nanotech.* **10,** 785–790 (2015).
13. Werber, J. R., Osuji, C. O. & Elimelech, M. Materials for next-generation desalination and water purification membranes. *Nat. Rev. Mater.* **1,** 16018 (2016).
14. Sahu, S., Ventra, M. D. & Zwolak, M. Dehydration as a universal mechanism for ion selectivity in graphene and other atomically thin pores. Preprint at http://arXiv.org/abs/1605.03134 (2016).
15. Richards, L. A., Schafer, A. I., Richards, B. S. & Corry, B. The importance of dehydration in determining ion transport in narrow pores. *Small* **8,** 1701–1709 (2012).
16. Thomas, M., Corry, B. & Hilder, T. A. What have we learnt about the mechanisms of rapid water transport, ion rejection and selectivity in nanopores from molecular simulation? *Small* **10,** 1453–1465 (2014).
17. Song, C. & Corry, B. Intrinsic ion selectivity of narrow hydrophobic pores. *J. Phys. Chem. B* **113,** 7642–7649 (2009).
18. Williams, C. D. & Carbone, P. Selective removal of technetium from water using graphene oxide membranes. *Environ. Sci. Technol.* **50,** 3875–3881 (2016).
19. Feng, J. *et al.* Observation of ionic Coulomb blockade in nanopores. *Nat. Mater.* **15,** 850–855 (2016).
20. Cohen-Tanugi, D., McGovern, R. K., Dave, S. H., Lienhard, J. H. & Grossman, J. C. Quantifying the potential of ultra-permeable membranes for water desalination. *Energy Environ. Sci.* **7,** 1134–1141 (2014).
21. Deshmukh, A., Yip, N. Y., Lin, S. H. & Elimelech, M. Desalination by forward osmosis: identifying performance limiting parameters through module-scale modeling. *J. Membr. Sci.* **491,** 159–167 (2015).
22. Das, R., Ali, M. E., Abd Hamid, S. B., Ramakrishna, S. & Chowdhury, Z. Z. Carbon nanotube membranes for water purification: a bright future in water desalination. *Desalination* **336,** 97–109 (2014).
23. Dreyer, D. R., Park, S., Bielawski, C. W. & Ruoff, R. S. The chemistry of graphene oxide. *Chem. Soc. Rev.* **39,** 228–240 (2010).
24. Wilson, N. R. *et al.* Graphene oxide: structural analysis and application as a highly transparent support for electron microscopy. *ACS Nano* **3,** 2547–2556 (2009).
25. Loh, K. P., Bao, Q., Eda, G. & Chhowalla, M. Graphene oxide as a chemically tunable platform for optical applications. *Nat. Chem.* **2,** 1015–1024 (2010).
26. Liu, H. Y., Wang, H. T. & Zhang, X. W. Facile fabrication of freestanding ultrathin reduced graphene oxide membranes for water purification. *Adv. Mater.* **27,** 249–254 (2015).
27. Sun, P. Z. *et al.* Highly efficient quasi-static water desalination using monolayer graphene oxide/titania hybrid laminates. *NPG Asia Mater.* **7,** e162 (2015).
28. Hu, M. & Mi, B. X. Enabling graphene oxide nanosheets as water separation membranes. *Environ. Sci. Technol.* **47,** 3715–3723 (2013).
29. Hung, W. S. *et al.* Cross-linking with diamine monomers to prepare composite graphene oxide-framework membranes with varying d-spacing. *Chem. Mater.* **26,** 2983–2990 (2014).
30. Zhang, Y., Zhang, S. & Chung, T. S. Nanometric graphene oxide framework membranes with enhanced heavy metal removal via nanofiltration. *Environ. Sci. Technol.* **49,** 10235–10242 (2015).
31. Greenspan, L. Humidity fixed-points of binary saturated aqueous-solutions. *J. Res. Natl Bur. Stand. Sect. A* **81,** 89–96 (1977).
32. Rezania, B., Severin, N., Talyzin, A. V. & Rabe, J. P. Hydration of bilayered graphene oxide. *Nano Lett.* **14,** 3993–3998 (2014).
33. Radha, B. *et al.* Molecular transport through capillaries made with atomic-scale precision. *Nature* **538,** 222–225 (2016).
34. Tissandier, M. D. *et al.* The proton's absolute aqueous enthalpy and Gibbs free energy of solvation from cluster ion solvation data. *J. Phys. Chem. A* **102,** 7787–7794 (1998).

35. Chekli, L. *et al.* A comprehensive review of hybrid forward osmosis systems: performance, applications and future prospects. *J. Membr. Sci.* **497,** 430–449 (2016).

Acknowledgements

This work was supported by the Royal Society and the Engineering and Physical Sciences Research Council, UK (EP/K016946/1 and EP/M506436/1). K.G. acknowledges Marie Curie International Incoming Fellowship. K.S.V. and R.R.N. acknowledge support from BGT Materials Limited.

Author contributions

R.R.N. designed and supervised the project with J.A. and K.S.V.; J.A. and K.S.V. prepared the samples, performed the measurements and carried out the analysis with help from R.R.N.; J.D., C.D.W. and P.C. carried out MD simulations and data analysis. K.G., Y.S. and C.T.C. helped in sample preparation, characterization and data analysis. E.P. and S.J.H. contributed to sample characterization. A.K.G. participated in discussions and project design. R.R.N., K.S.V., J.A., C.D.W., I.V.G. and A.K.G. wrote the manuscript. All authors contributed to discussions.

Additional information

Supplementary information is available in the online version of the paper. Reprints and permissions information is available online at www.nature.com/reprints. Correspondence and requests for materials should be addressed to R.R.N.

Competing financial interests

The authors declare no competing financial interests.

Methods

Preparation of GO membranes. The aqueous suspension of graphene oxide (GO) was prepared by dispersing millimetre-sized graphite oxide flakes (purchased from BGT Materials Limited) in distilled water using bath sonication for 15 h. The resulting dispersion was centrifuged 6 times at 8,000 r.p.m. to remove the multilayer GO flakes. Subsequently, freestanding GO membranes of thickness ≈100 μm were prepared by vacuum filtration of supernatant GO suspension[4] through an Anodisc alumina membrane filter (0.2 μm pore size and a diameter of 47 mm, purchased from Millipore). As-prepared GO membranes were dried in an oven for 10 h at 45 °C and cut into rectangular strips of dimension of 4 mm × 10 mm (Supplementary Fig. 1).

Tuning interlayer spacing in GO laminates. GO membranes with different interlayer spacing were prepared by storing them in a sealed container with different RH of 0, 12, 33, 75, 84 and 100%. To this end, we used saturated solutions of LiCl (12% RH), $MgCl_2$ (33% RH), NaCl (75% RH) and KCl (84% RH), which were prepared by dissolving excess amounts of salts in deionized water[31,36]. A humidity meter was used inside the container to check that the salts provided the literature values of RH. As a zero humidity environment, we used a glove box filled with Ar and H_2O content below 0.5 p.p.m. 100% RH was achieved inside a sealed plastic container filled with a saturated water vapour at room temperature.

Analysis of the interlayer spacing. X-ray diffraction (XRD) measurements in the 2θ range 5° to 15° (with a step size of 0.02° and recording rate of 0.1 s) were performed using a Bruker D8 diffractometer with Cu Kα radiation ($\lambda = 1.5406$ Å). To collect an XRD spectrum from a GO membrane stored at a specific RH, we created the same humid environment inside a specimen holder (Bruker, C79298A3244D83/85) and sealed it with the GO membrane. For the case of zero humidity, an airtight sample holder (Bruker, A100B36/B37) was used. All spectra were taken with a short scanning time to avoid possible hydration/dehydration of the GO membranes. From XRD analysis of the (001) reflection, d for 0, 12, 33, 75, 84 and 100% RH are found to be 6.4, 7.4, 7.9, 8.6, 9 and 9.8 Å, respectively.

Fabrication of PCGO membranes. After achieving the desired d by using different humidities, each rectangular strip was immediately glued and stacked with Stycast 1266. This stack was then immediately transferred to the same humid environment (where the GO laminates were initially stored) for curing the epoxy overnight. Finally, the resulting stacks were glued into a slot in a plastic or copper plate as shown in Fig. 1. An epoxy layer present at the top and bottom cross-sections of the glued stacks was carefully cleaved to produce a clean surface for permeation experiments. The cleaved cross-section was also checked under an optical microscope to remove any possible epoxy residues. The entire fabrication procedure is illustrated in Supplementary Fig. 1. Swelling of the PCGO membranes on exposure to liquid water was monitored by measuring the cross-sectional thickness of the membranes in an optical microscope immediately after and before performing the ion permeation experiments. The increase in thickness after the permeation experiments was found to be <1%, indicating negligible swelling of PCGO membranes. Similarly, the effect of epoxy encapsulation on d was monitored by measuring the thickness of GO laminates before and after encapsulation. No changes were found. We also carried out an additional check in which the epoxy encapsulation was removed around one of the GO membranes ($d \approx 7.9$ Å) and X-ray measurements were immediately performed. No change in d (with accuracy of 1–2%) was observed, which confirms the stability of d after the encapsulation procedure.

Permeation experiments. All permeation measurements were carried out using the set-up shown in Supplementary Fig. 2, which consists of feed and permeate compartments made from Teflon. PCGO membranes incorporated plastic or metal plates (Supplementary Fig. 1) were clamped between two O-rings and then fixed between the feed and permeate compartments to provide a leak tight environment for the permeation experiments. We filled the compartments with equal volumes (10 ml) of a salt solution (feed) and deionized water (permeate) to avoid any hydrostatic pressure due to different heights of the liquids. Permeation experiments at different temperatures (2–43 °C) were performed in a temperature-controlled environmental chamber. The measurement set-up, feed and permeate solutions were equilibrated at each temperature before performing the experiment. Magnetic stirring was used in both compartments to avoid concentration polarization effects. Anion and cation concentrations in the permeate compartment caused by diffusion through PCGO membranes were accurately measured using ion chromatography (IC) and inductively coupled plasma atomic emission spectrometry (ICP-AES) techniques[4]. Using the known volume of the permeate compartment, the concentrations allowed us to calculate the amount of ions that diffused into it.

Data availability. The data that support the plots within this paper and other findings of this study are available from the corresponding author upon reasonable request. Data related to molecular dynamics simulations are available from P.C. (Paola.Carbone@manchester.ac.uk).

References

36. Rockland, L. B. Saturated salt solutions for static control of relative humidity between 5° and 40° C. *Anal. Chem.* **32,** 1375–1376 (1960).